Biophysical Chemistry 141 (2009) 49–58

Contents lists available at ScienceDirect

Biophysical Chemistry

journal homepage: http://www.elsevier.com/locate/biophyschem

Investigation of intermolecular hydrogen bond interactions in crystalline L-Cysteine by DFT calculations of the oxygen-17, nitrogen-14, and hydrogen-2 EFG tensors and AIM analysis

Ahmad G. Nozad [a,*], Sakineh Meftah [b], Mohammad H. Ghasemi [b], Roya A. Kiyani [b], Mustafa Aghazadeh [b,c,*]

[a] Material Research School, NSTRI, P.O. Box:14395-836, Tehran, Iran
[b] Applied Chemistry Research Group, ACECR–Tehran branch, P.O. Box: 13145-186, Tehran, Iran
[c] Department of Chemistry, Tarbiat Modares University, P.O. Box:13145-185, Tehran, Iran

ARTICLE INFO

Article history:
Received 3 November 2008
Received in revised form 21 December 2008
Accepted 21 December 2008
Available online 7 January 2009

Keywords:
L-Cysteine
Hydrogen bond interactions
Density functional theory
Electric field gradient tensor
Asymmetry parameter
AIM analysis

ABSTRACT

A systematic computational study is carried out to investigate hydrogen bond (HB) interactions in the real crystalline structures of L-Cysteine at 30 and 298 K by density functional theory (DFT) calculations of electric field gradient (EFG) tensors at the sites of O-17, N-14, and H-2 nuclei. One-molecule (monomer) and nine-molecule (cluster) models of L-Cysteine are created by available crystal coordinates at both temperatures and the EFG tensors are calculated for both models to indicate the effect of HB interactions on the tensors. The calculated EFG tensors at the level of B3LYP and B3PW91 DFT methods and 6-311++G** and cc-pVTZ basis sets are converted to those experimentally measurable nuclear quadrupole resonance (NQR) parameters i.e. quadrupole coupling constants (qcc) and asymmetry parameters (η_Q). The evaluated NQR parameters reveal that the EFG tensors of ^{17}O, ^{14}N, and ^{2}H are influenced and show particular trends from monomer to the target molecule in the cluster due to the contribution of target molecule to classic N–H…O, and non-classic S–H…O and S–H…S types of HB interactions. On the other hand, atoms in molecules (AIM) analyses confirm the presence of HB interactions and rationalize the observed EFG trends. The results indicate different contribution of various nuclei to HB interactions in the cluster where O2 and N1 have major contributions. The EFG tensors as well as AIM analysis at the H6 site show that the N1-H6…O2 HB undergoes a significant change from 30 to 298 K where changes in other N–H…O interactions are almost negligible. There is a good agreement between the calculated ^{14}N NQR parameters and reported experimental data.

1. Introduction

Hydrogen bond (HB) interactions are crucial elements in the biochemical activities, and determination and stabilization of the three-dimensional structures of biological systems [1,2]. Moreover, HBs play an important role in studying structural molecular biology [3–5]. Due to the importance, the nature of these interactions has been extensively investigated by numerous either experimental or theoretical studies [6–12]. To have a better determination of the HB properties, nuclear quadrupole resonance (NQR) spectroscopy is among the most important and versatile techniques for this purpose. NQR parameters being very sensitive to HBs are useful elements in the study of hydrogen-bonded systems. Since the most characteristic nature of HB interactions is electrostatic, electric field gradient (EFG) tensors originated at the sites of quadrupole nuclei are proper elements to characterize the HB interactions in solid phase [13–15]. It is noted that quadrupole nuclei are those with spin angular moment greater than one-half ($I>1/2$) which the interaction energy of the nuclear electric quadrupole moment (eQ) and the EFG tensors is measured by NQR as a quadrupole coupling constant (qcc). Asymmetry parameter (η_Q) indicating the EFG tensors deviation from cylindrical symmetry at the site of quadrupole nucleus is also measured by NQR.

The application of the Atoms and Molecules Theory to understand the nature of the bonds such as HBs in deeper detail is an interesting approach and several excellent reviews have been published on the theory of Atoms in Molecules (AIM) developed by Bader [16–18]. Also, the analysis of the critical points (CP) of the distribution of the electronic density has demonstrated to be a potentially useful tool to study different significant chemical features such as the structure, nature, and geometry of hydrogen-bonded systems [19–22]. Thus, this analysis is used as well as EFG calculations for study of the HB interactions properties in L-Cysteine. Previously, Matta and Bader [23–25] have also studied the bond and atomic properties of amino

* Corresponding authors. Nozad is to be contacted at Material Research School, NSTRI, P.O. Box:14395-836, Tehran, Iran. Tel.: +98 21 8206 3118; fax: +98 21 8206 3112. Aghazadeh, Department of Chemistry, Tarbiat Modares University, P.O. Box:13145-185, Tehran, Iran. Tel.: +98 21 61113335.
E-mail addresses: anozad@aeoi.org.ir (A.G. Nozad), m_aghazadeh@modares.ac.ir (M. Aghazadeh).

0301-4622/$ – see front matter © 2008 Elsevier B.V. All rights reserved.
doi:10.1016/j.bpc.2008.12.013

acids conformers and the effect of conformation and tautomerization on these properties by using AIM theory.

Study the properties of HB interactions in amino acids and derivatives is an interesting subject due to their key role in secondary and tertiary structures of proteins. Furthermore, understanding the nature of these interactions can be a crucial step to describe the functionality of these systems in biological media at molecular level. L-Cysteine ($SH–CH_2–CH_2–NH_2COOH$) carrying an amino, a carboxylic acid, and a thiol group is capable of donating and accepting intramolecular HBs. L-Cysteine thiol or sulfhydryl (S–H) groups can contribute to the stabilization of native protein structures since they are highly polarizable and the most chemically reactive sites in proteins under physiological conditions [26–29]. The Cysteine sulfhydryl may function as either a HB donor (e.g., S–H…O) or an acceptor (e.g., H…S–H) group. Sulfhydryl HB in proteins is not well understood, primarily because such HB interactions are difficult to detect experimentally due to their weakness. L-Cysteine like all amino acids exists in gas phase mainly as neutral form but in solution and solid phase chiefly as zwitterions-neutral form with charge separation. Both X-ray and neutron diffraction studies have been carried out to characterize the HBs of the L-Cysteine crystalline structure [30–37]. These studies have revealed that L-Cysteine occurs in the crystals in the dipolar ion (zwitterions) form and the amino and thiol group hydrogen atoms participate in a three-dimensional network of HBs. Based on these studies, in solid phase, L-Cysteine crystallizes into two different polymorphs, orthorhombic [30–33] and monoclinic [34–37], which are characterized by the presence of one and two molecules of L-Cysteine in the asymmetric unit, respectively. As evidenced by X-ray [31] and neutron diffraction [32], at ambient temperature, the sulfur atoms of the thiol groups are disordered over two positions. The distances between the oxygen and sulfur atoms of the neighboring molecules in the structure are consistent with the hypothesis on the formation of the two types of intermolecular HBs (S–H…S and S–H…O). A recent structural study of L-Cysteine at 30 K [30] has shown the sulfur atoms to be completely ordered and located at those positions, which correspond to the formation of the S–H…S HBs.

The previous quantum mechanical calculations on L-Cysteine include studies of protonation and ionization potential [38], a comparison of PCILO and SCF results [39], grand state vibrational spectra [40,41], minimum energy conformations [42,43], and electronic excitations of Cysteine conformers [44]. Recently, Pawlukojc et al. [45] have carried out neutron spectroscopy, Raman, IR, and ab initio calculations on L-Cysteine. Their work suggests that the presence of a three-dimensional network of HBs affects the structural and dynamical parameters of the molecule in the crystal to such extent that the "free molecule" approximation reflects the geometry of the L-Cysteine

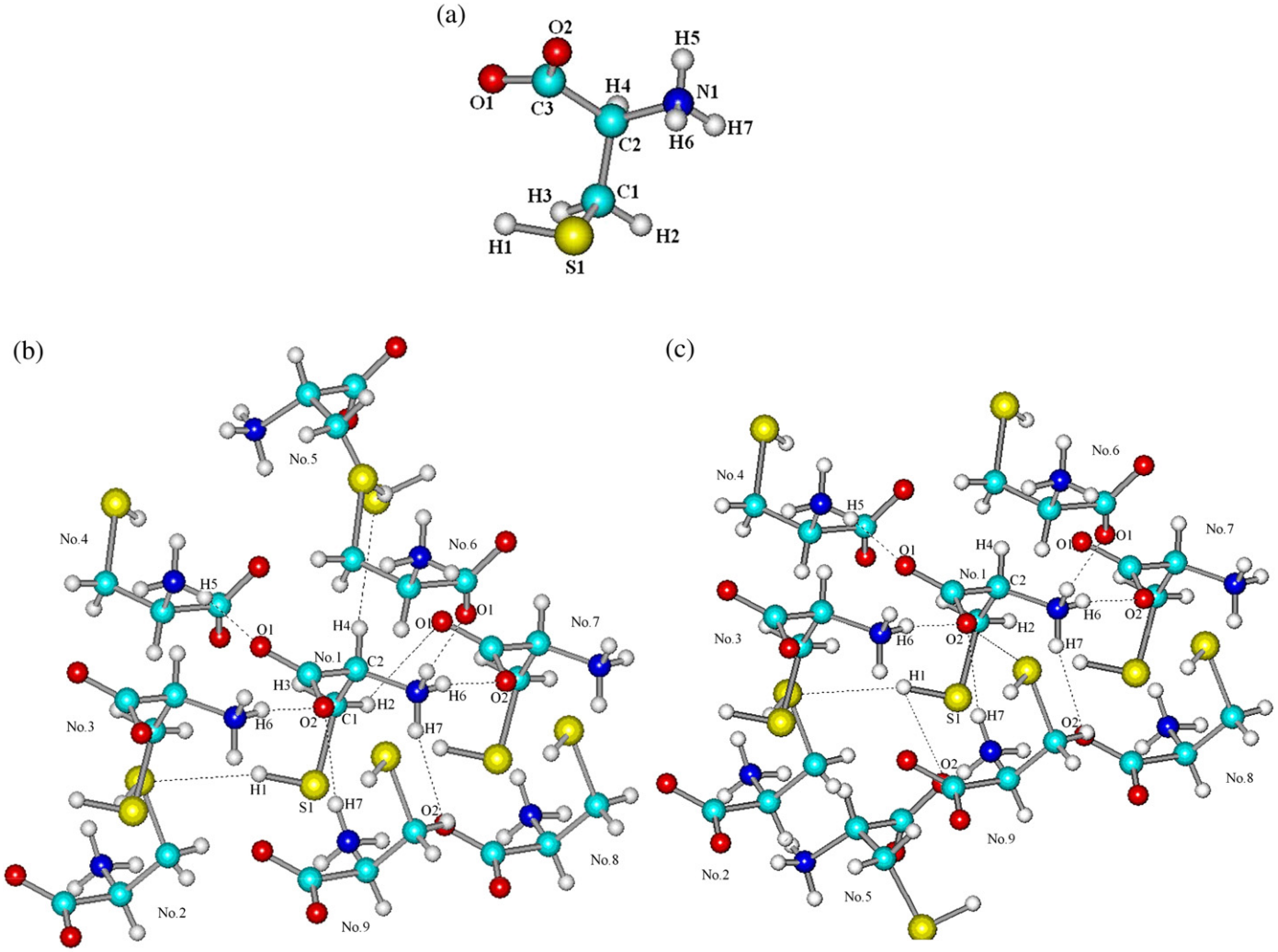

Fig. 1. (a) Monomer, and (b) and (c) nine-molecule clusters of L-Cysteine at 30 and 298 k, respectively. No.1 (Target molecule): (x,y,z); No.2: ($1/2-x,2-y,-1/2+z$); No.3: ($3/2-x,2-y,1/2+z$); No.4: ($1/2+x,3/2-y,1-z$); No.5: ($1-x,-1/2+y,3/2-z$); No.6: ($x,y,1+z$); No.7: ($1+x,y+1/2,z$); No.8: ($x+1/2,y,z$); No.9: ($-1/2+x,y,z$). At 298 K, No.5: ($-1/2+x,1-yz-1/2$). Dashed lines show the HBs (Table 2).

Table 1
The structural properties of L-Cysteine

Geometrical parameters	Monomer at 30 K[a]	Monomer at 30 K[b]	Cluster at 30 K[c]	Cluster at 298 K[d]	Cluster at 298 K[e]
S1-H1	1.303 Å	1.301 Å	1.391 Å	1.452 Å	1.371 Å
C1-H2	0.961 Å	1.069 Å	1.070 Å	1.077 Å	1.077 Å
C1-H3	0.987 Å	1.054 Å	1.141 Å	1.076 Å	1.076 Å
C2-H4	0.932 Å	1.071 Å	1.096 Å	1.104 Å	1.104 Å
N1-H5	0.825 Å	1.004 Å	1.070 Å	1.038 Å	1.038 Å
N1-H6	0.866 Å	0.998 Å	1.051 Å	1.027 Å	1.027 Å
N1-H7	0.894 Å	1.011 Å	1.076 Å	1.065 Å	1.065 Å
S1-C1	1.824 Å	1.824 Å	1.824 Å	1.791 Å	1.812 Å
C1-C2	1.522 Å	1.523 Å	1.523 Å	1.529 Å	1.529 Å
C2-N1	1.484 Å	1.484 Å	1.485 Å	1.488 Å	1.488 Å
C3-O1	1.244 Å	1.244 Å	1.244 Å	1.239 Å	1.239 Å
C3-O2	1.262 Å	1.262 Å	1.262 Å	1.251 Å	1.251 Å
∠S1-C1-C2	113.91°	113.91°	113.91°	114.83°	112.32°
∠S1-C1-H2	108.03°	107.21°	110.01°	107.35°	109.60°
∠C1-C2-C3	111.07°	111.07°	110.07°	111.12°	111.12°
∠C2-N1-H5	107.92°	108.14°	105.21°	110.63°	110.63°
∠O1-C3-C2	117.01°	117.05°	117.05°	117.02°	117.02°
∠O2-C3-C2	116.91°	116.91°	116.91°	117.32°	117.32°
∠O1-C3-O2	126.07°	126.08°	126.01°	125.71°	125.71°
∠H7-N1-H5	108.32°	110.24°	111.31°	108.04°	108.04°
∠H6-N1-H5	111.62°	107.34°	109.17°	108.74°	108.74°
∠H7-N1-H6	108.33°	109.23°	112.03°	106.84°	106.83°

[a] Data from Ref. [30].
[b] Crystalline monomer is obtained by X-ray coordinates [30], and H-optimization is also performed.
[c] Target molecule in cluster model where H-optimization is also carried out.
[d] Target molecule in cluster model, data from Ref. [32].
[e] Target molecule in cluster where partial optimization is also performed.

molecule in the crystal only in limited scope. Scheiner et al. [46] studied the strength of the C^{α}–H…O HB of amino acid residues by performing ab initio calculations of C^{α}–H group binding energy to a water molecule. They concluded that the C^{α}–H…O interaction appears to be a true HB and must be considered as a potentially important factor in protein structure and function. Hadipour et al. [47,48] using DFT calculations have shown that ^{14}N, ^{17}O, and ^{2}H NQR parameters in amino acids are sensitive to the lattice effects such as HB interactions and appropriate to characterize the property of these interactions. Also, the correlation between NQR parameters and residue size of aliphatic amino acids and their dimers have been studied by Ghaderi et al. [49]. During the 1970s, many of the amino acids were investigated Experimentally by ^{14}N NQR spectroscopy [50–54], and several of their ^{14}N quadrupolar coupling parameters (qcc (^{14}N)≈1.2 MHz) were determined. Also, the solid state ^{17}O NMR of amino acids was studied by Pike et al. [55], and the NQR interaction parameters for amino acids showed a wide variation of qcc, from 6.4 to 8.6 MHz, η_Q, from 0.0 to 0.9. Recently, the ^{14}N NQR parameters of L-Cysteine (qcc(^{14}N)=1.22 MHz and η_Q=0.5) were reported by Giavani et al. [56].

The present work includes a systematic computational study of the properties of HB interactions in the crystalline structures of L-Cysteine at 30 and 298 K via density functional theory (DFT) calculations of the ^{17}O, ^{14}N, and ^{2}H EFG tenors and AIM analysis of charge density where the crystalline coordinates of L-Cysteine are obtained from X-ray and neutron diffraction studies [30,32]. To calculate reliable EFG results, the considered model system in calculations must be as much closer to experiment as possible [57–63]. Since L-Cysteine contributes to HB interactions in the solid phase (N–H…O, S–H…O and S–H…S types), the most possible interacting molecules with the central molecule are considered via a nine-molecule (cluster) model; see Fig. 1 and Tables 1 and 2 for details. To have a basis for comparison of HBs effects on the EFG tensors, the calculations are also performed on the monomer of L-Cysteine at both temperatures. All calculations are carried out at B3LYP and B3PW91 levels using 6-311++G(d,p) and cc-pVTZ basis sets. The calculated EFG tensors at the sites of ^{17}O, ^{14}N, and ^{2}H nuclei are converted to the experimentally measurable NQR parameters (qcc and η_Q) which are exhibited in Tables 3 and 4. Finally, AIM analyses are performed on wave functions of L-Cysteine at 30 and 298 K obtained from Gaussian output, the results are exhibited in Tables 5 and 6.

2. Methods and computational details

Two methods are chosen for investigation of intermolecular HB interactions in crystalline L-Cysteine; DFT calculations of the oxygen-17, nitrogen-14, and hydrogen-2 EFG tensors and topological analysis of charge density at the bond critical points via AIM theory which are separately discussed in two sections.

Table 2
Geometrical parameters of intermolecular HB interactions of L-Cysteine (Å, °)

r[target…neighbor][a]	30 K[b]	30 K[c]	298 K[d]	∠ [N–H…O][a]	30 K[b]	30 K[c]	298 K[d]
N1–H5…O(1–6)	1.97	1.73	1.77	N1–H5…O(1–6)	162.14	165.67	164.54
N1–H6…O(2–7)	2.12	1.86	2.06	N1–H6…O(2–7)	159.14	165.71	156.36
N1–H7…O(2–8)	1.87	1.65	1.71	N1–H7…O(2–8)	169.62	173.25	174.11
S1–H1…S(1–2)	2.66	2.64	2.63(2.59)	S1–H1…S(1–2)	150.81	150.45	140.26(143.12)
C1–H2…O(1–7)	2.56	2.25	–	C1–H2…O(1–7)	132.66	133.74	–
C2–H4…S(1–5)	2.85	2.66	–	C2–H4…S(1–5)	175.48	174.17	–
O1…H–N(1–4)	1.97	1.73	1.77	O1….H–N(1–4)	162.14	164.39	164.52
O2…H–N(1–3)	2.12	1.86	2.06	O2….H–N(1–3)	159.14	158.79	156.87
O2…H–N(1–9)	1.87	1.65	1.71	O2….H–N(1–9)	169.63	175.48	174.11
S1–H1…O(2–5)	–	–	2.40(2.43)	S1–H1…O(2–5)	–	–	134.76(132.31)
S1…S(1–2)	3.85	3.85	3.79(3.81)				
N1…O(1–6)	2.77	2.77	2.78				
N1…O(2–7)	2.94	2.94	3.02				
N1…O(2–8)	2.75	2.75	2.74				
C1…O(1–7)	3.27	3.27	–				
C2…S(1–5)	3.77	3.77	–				
S1…O(2–5)	–	–	3.41(3.45)				
O1…N(1–4)	2.77	2.77	2.78				
O2…N(1–3)	2.93	2.93	3.02				
O2…N(1–9)	2.75	2.75	2.76				

[a] The first number in parentheses denotes the atom number and the second one donates the molecule number (see Fig. 1).
[b] Data from X-ray study [30].
[c] Cluster is obtained by X-ray coordinates [30], and H-optimization is also performed at the level of B3LYP/6-311++G(d,p).
[d] Data from neutron diffraction study [32] where the results in parentheses are obtained from partial optimization of cluster.

Table 3
The calculated O-17 and N-14 quadrupole coupling tensors (qcc) and asymmetry parameters (η_Q) for crystalline L-Cysteine at 30 and 298 K

Nucleus	Methods	Basis sets	30 K		298 K	
			qcc(MHz)[a]	η_Q[a]	qcc(MHz)[a]	η_Q[a]
O(1)	B3PW91	6-311++G**	7.53(7.69)	0.51(0.37)	7.39(7.48)	0.54(0.41)
		cc-pVTZ	7.61(7.64)	0.49(0.36)	7.35(7.49)	0.51(0.42)
	B3LYP	6-311++G**	7.54(7.67)	0.52(0.34)	7.37(7.47)	0.55(0.45)
		cc-pVTZ	7.59(7.69)	0.50(0.36)	7.38(7.49)	0.54(0.42)
O(2)	B3PW91	6-311++G**	8.21(8.69)	0.41(0.31)	8.12(8.44)	0.48(0.35)
		cc-pVTZ	8.29(8.61)	0.44(0.33)	8.15(8.41)	0.49(0.37)
	B3LYP	6-311++G**	8.26(8.67)	0.42(0.34)	8.14(8.42)	0.45(0.37)
		cc-pVTZ	8.26(8.65)	0.44(0.31)	8.17(8.44)	0.46(0.37)
N(1)	B3PW91	6-311++G**	1.24(0.69)	0.68(0.22)	1.20 (0.84)	0.37(0.14)
		cc-pVTZ	1.25(0.61)	0.64(0.31)	1.18(0.79)	0.34(0.16)
	B3LYP	6-311++G**	1.28(0.66)	0.67(0.28)	1.21(0.86)	0.39(0.18)
		cc-pVTZ	1.27(0.64)	0.69(0.24)	1.19(0.81)	0.35(0.15)
Exp.[b]					1.22	0.50

[a] The calculated results out of parentheses are for the target molecule in nine-molecule cluster, and those are in parentheses are for monomer.
[b] Experimental values of N-14 at 298 K from Ref. [56].

2.1. DFT calculations of EFG tensors

The quantum mechanical calculations of EFG tensors at the oxygen, nitrogen, and hydrogen sites of L-Cysteine are carried out at the level of DFT by employing the Gaussian 98 package [64]. Köster et al. [65–67] have also showed that DFT calculations are capable to reliably predict ^{14}N and ^{17}O NQR frequencies and their nuclear quadrupole coupling constants. The crystalline structures of L-Cysteine at 30 and 298 K are obtained from X-ray and neutron diffraction studies, respectively, [30,32]. Since the positions of hydrogen atoms are not located accurately by X-ray diffraction, a geometry optimization of just hydrogen atoms (H-optimization) in the structure is needed at 30 K. The H-optimization is performed at the B3LYP/6-311++G(d,p) level, where during this optimization the positions of the hydrogen atoms are allowed to fully relax while those of other atoms remained frozen. It should be noted that the position of hydrogen atoms are determined accurately by neuron diffraction, thus, no geometry optimization is needed for L-Cysteine crystalline structure at 298 K. However, partial optimization is carried out for S and H atoms in the monomer and the cluster since it has been demonstrated [32] that these atoms are disordered at 298 K. For both L-Cysteine crystalline structures, nine-molecule clusters involving the most probable interacting molecules with the target molecule are created using coordinate transformation and are considered in the calculations; see Fig. 1 and Tables 1 and 2.

To calculate ^{17}O, ^{14}N, and ^{2}H EFG tensors in the principal axis system (PAS), two level of DFT methods including B3LYP and B3PW91 [68–70] with the basis sets of 6-311++G(d,p) and cc-pVTZ are employed. These basis sets are chosen since various combinations of diffuse and polarization functions being necessary for computation of EFG tensors of hydrogen, nitrogen and oxygen atoms involved in HBs are included in 6-311++G** basis set [71,72]. Furthermore, pervious experiences reveal that these two basis sets usually lead to satisfactory EFG values [57–63].

To have a comparison among the capabilities of various nuclei in contribution to HB interactions, and also to systematically investigate the HB effects on the ^{17}O, ^{14}N, and ^{2}H EFG tensors in L-Cysteine crystalline structures, all the calculations are performed for both forms of the crystalline monomer and the nine-molecule cluster of L-Cysteine at both mentioned temperatures; see Tables 3 and 4. To compare the calculated EFG tensors with experimental quadrupole parameters, the following equation is used to convert the EFG tensor components, q_{ii}, in atomic units (a.u.) to the quadrupole coupling constant, qcc, in MHz:

$$\mathrm{qcc(MHz)} = e^2 Q q_{zz} h^{-1} \quad (1)$$

where Q is the nuclear quadrupole moment of the ^{17}O, ^{14}N, and ^{2}H nuclei. In this work, the reported standard Q value by Pyykkö [73] are used, $Q(^{17}O)=25.58$ mb, $Q(^{14}N)=20.44$ mb, and $Q(^{2}H)=2.86$ mb.

Table 4
Calculated H-2 quadrupole coupling tensors (qcc) and asymmetry parameters (η_Q) for crystalline L-Cysteine

Nucleus	Methods	Basis sets	30 K		298 K	
			qcc(MHz)[a]	η_Q[a]	qcc (MHz)[a]	η_Q[a]
H(1)	B3PW91	6-311++G**	192.3 (199.7)	0.09 (0.08)	179.3 (194.1)	0.1 (0.07)
		cc-pVTZ	192.7 (200.4)	0.09 (0.08)	177.7 (194.8)	0.1 (0.05)
	B3LYP	6-311++G**	191.7 (201.4)	0.1 (0.08)	178.4 (193.1)	0.09 (0.02)
		cc-pVTZ	193.4 (200.5)	0.1 (0.08)	177.6 (194.1)	0.09 (0.03)
H(2)	B3PW91	6-311++G**	211.5 (222.2)	0.1 (0.09)	226.9 (228.8)	0.09 (0.08)
		cc-pVTZ	209.5 (219.2)	0.09 (0.08)	224.6 (225.1)	0.09 (0.07)
	B3LYP	6-311++G**	209.7 (220.8)	0.1 (0.09)	227.1 (228.4)	0.1 (0.08)
		cc-pVTZ	210.3 (217.4)	0.1 (0.08)	223.3 (225.1)	0.1 (0.07)
H(3)	B3PW91	6-311++G**	194.1 (195.7)	0.05 (0.02)	201.5 (201.1)	0.02 (0.01)
		cc-pVTZ	194.6 (195.3)	0.05 (0.02)	204.7 (204.2)	0.03 (0.01)
	B3LYP	6-311++G**	198.9 (200.4)	0.05 (0.03)	201.6 (202.2)	0.02 (0.01)
		cc-pVTZ	199.1 (200.2)	0.05 (0.03)	200.8 (202.7)	0.02 (0.01)
H(4)	B3PW91	6-311++G**	192.5 (197.4)	0.09 (0.04)	205.4 (207.3)	0.01 (0.00)
		cc-pVTZ	195.1 (197.5)	0.09 (0.02)	204.7 (206.1)	0.01 (0.00)
	B3LYP	6-311++G**	194.1 (198.6)	0.1 (0.05)	203.6 (204.5)	0.05 (0.02)
		cc-pVTZ	193.7 (197.2)	0.09 (0.07)	203.7 (204.6)	0.02 (0.00)
H(5)	B3PW91	6-311++G**	161.3 (185.4)	0.04 (0.02)	173.3 (196.4)	0.03 (0.00)
		cc-pVTZ	160.9 (184.9)	0.02 (0.01)	172.6 (195.3)	0.04 (0.00)
	B3LYP	6-311++G**	162.7 (186.7)	0.05 (0.02)	171.4 (194.5)	0.05 (0.01)
		cc-pVTZ	165.1 (187.3)	0.02 (0.00)	170.3 (195.6)	0.04 (0.00)
H(6)	B3PW91	6-311++G**	202.2 (219.7)	0.01 (0.00)	199.1 (204.4)	0.03 (0.00)
		cc-pVTZ	207.7 (218.4)	0.02 (0.00)	191.7 (205.7)	0.02 (0.01)
	B3 LYP	6-311++G**	203.9 (220.3)	0.03 (0.01)	196.9 (207.5)	0.03 (0.01)
		cc-pVTZ	209.1 (224.9)	0.01 (0.00)	198.6 (209.5)	0.02 (0.01)
H(7)	B3PW91	6-311++G**	150.4 (179.1)	0.03 (0.01)	159.1 (182.4)	0.03 (0.01)
		cc-pVTZ	149.4 (178.8)	0.03 (0.01)	158.7 (189.8)	0.02 (0.01)
	B3LYP	6-311++G**	145.2 (172.5)	0.02 (0.01)	160.1 (186.7)	0.03 (0.02)
		cc-pVTZ	147.3 (175.6)	0.02 (0.01)	158.2 (184.3)	0.04 (0.02)

[a] The calculated results out of parentheses are for the target molecule in cluster, and those are in parentheses are for monomer.

Another important NQR parameter is the asymmetry parameter (η_Q) which measures the EFG tensors deviation from axial symmetry at the site of quadrupole nucleus, is obtained by Eq. (2).

$$\eta_Q = \left|\frac{q_{yy}-q_{xx}}{q_{zz}}\right|, \quad 0 \le \eta_Q \le 1 \tag{2}$$

The calculated ^{17}O, ^{14}N, and ^{2}H qcc and η_Q parameters for crystalline monomer and the target molecule in crystalline cluster of L-Cysteine at 30 and 298 K are exhibited in Tables 3 and 4.

2.2. AIM theory and calculations

AIM theory [16] is based on the critical points (CPs) of the molecular electronic charge density,$\rho(r)$. These are points where the electronic density gradient ($\nabla^2\rho(r)$) vanishes and which are characterized by the three eigenvalues (λ_i, i=1,2,3) of the Hessian matrix of $\rho(r)$. λ_1, λ_2 correspond to the perpendicular curvatures and λ_3 provides a curvature along the internuclear axis. The CPs are labeled (r,s) according to their rank, r (number of non-zero eigenvalues), and signatures (the algebraic sum of the signs of λ_i). Four types of CPs are of interest in molecules: (3,+3), (3,+1), (3,−3) and (3,−1).

A (3,−1) point or bond critical point (BCP) is generally found between two neighboring nuclei indicating the existence of a bond between them. The Laplacian of charge density at the BCP ($\nabla^2\rho_{BCP}$) is the sum of the curvatures in the electron density along any orthogonal coordinate axes at the BCP. The sign of $\nabla^2\rho_{BCP}$ indicates whether the charge density is locally depleted ($\nabla^2\rho_{BCP}>0$) or locally concentrated ($\nabla^2\rho_{BCP}<0$). Thus, when the negative curvatures i.e. λ_1 and λ_2 dominate at the BCP, the electronic charge is locally concentrated within the region inter atoms leading to an interaction named as covalent or polarized bonds and being characterized by large ρ_{BCP} values, $\nabla^2\rho_{BCP}<0$, and $|\lambda_1|/\lambda_3>1$. On the other hand, if the positive curvature i.e. λ_3 is dominant, the electronic density is locally concentrated in each of the atomic basins. The interaction is now referred to as a closed-shell and it is characteristic of highly ionic bonds, HBs and van der Waals interactions. It is characterized by relatively low ρ_{BCP} values, $\nabla^2\rho_{BCP}>0$, and $|\lambda_1|/\lambda_3<1$.

Another interesting parameter is the ellipticity (ε) defined as $(\lambda_1/\lambda_2)-1$. It is indicative of the similarity between the perpendicular curvatures (λ_1 and λ_2) at the BCP. In terms of the orbital model of electronic structure, the ellipticity provides a quantitative measure of the π-bond character and of the delocalization electronic charge. Also, ellipticity is a measure of bond stability; high ellipticity values indicate instability of the bond [16–18].

For AIM analysis, wave functions of H-optimized (at the level of B3LYP/6-311++G**) crystalline clusters of L-Cysteine at 30 and 298 are generated from Gaussian output files at the level of B3LYP/6-311++G**.

Table 5
BCP properties for HB interactions in L-Cysteine crystalline structure at 30 K[a]

HB type [b]	ρ_{BCP}	$\nabla^2\rho_{BCP}$	$-\lambda_1$	$-\lambda_2$	λ_3	ε	$\lvert\lambda_1\rvert/\lambda_3$
H(1–1)…S (1–2)	0.0141	0.0418	0.0136	0.0129	0.0683	0.0529	0.1991
H(2–1)…O(1–7)	0.0102	0.0359	0.0099	0.0086	0.0544	0.1511	0.1819
H(4–1)…S (1–5)	0.0097	0.0331	0.0093	0.0082	0.0506	0.1341	0.1838
H(5–1)…O(1–6)	0.0342	0.1451	0.0547	0.0539	0.2536	0.0148	0.2157
H(6–1)…O(2–7)	0.0222	0.0952	0.0303	0.0283	0.1538	0.0706	0.1971
H(7–1)…O(2–8)	0.0450	0.1617	0.0794	0.0759	0.3171	0.0461	0.2504
H(5–4)…O(1–1)	0.0343	0.1454	0.0546	0.0538	0.2541	0.0148	0.2148
H(6–3)…O(2–1)	0.0222	0.0951	0.0303	0.0283	0.1537	0.0706	0.1971
H(7–9)…O(2–1)	0.0451	0.1618	0.0795	0.0759	0.3171	0.0474	0.2506

[a] All λ_i, ρ_{BCP} and $\nabla^2\rho_{BCP}$ values are in atomic unit.
[b] The first number in parentheses denotes the atom number and the second one donates the molecule number, for example, H(1–1) donates H1 of molecule number one in cluster model (see Fig. 1b and Table 2).

Table 6
BCP properties for HB interactions in L-Cysteine crystalline structure at 298 K[a]

HB type [b]	ρ_{BCP}	$\nabla^2\rho_{BCP}$	$-\lambda_1$	$-\lambda_2$	λ_3	ε	$\lvert\lambda_1\rvert/\lambda_3$
H(1–1)…S (1–2)	0.0124	0.0388	0.0114	0.0102	0.0615	0.1176	0.1886
H(1–1)…O (2–5)	0.0146	0.0615	0.0173	0.0161	0.0949	0.0745	0.1823
H(5–1)…O (1–6)	0.0318	0.1116	0.0468	0.0446	0.2029	0.0493	0.2306
H(6–1)…O (2–7)	0.0101	0.0403	0.0114	0.0105	0.0623	0.0857	0.1829
H(7–1)…O (2–8)	0.0448	0.1528	0.0789	0.0757	0.3075	0.0422	0.2565
H(5–4)…O (1–1)	0.0318	0.1116	0.0468	0.0446	0.2029	0.0493	0.2306
H(6–3)…O (2–1)	0.0102	0.0403	0.0114	0.0106	0.0623	0.0755	0.1829
H(7–9)…O (2–1)	0.0448	0.1528	0.0789	0.0757	0.3075	0.0422	0.2565
H(1–9)…O (2–1)	0.0146	0.0615	0.0173	0.0161	0.0949	0.0745	0.1823

[a] All λ_i, ρ_{BCP} and $\nabla^2\rho_{BCP}$ values are in atomic unit.
[b] The first number in parentheses denotes the atom number and the second one donates the molecule number, for example, O(2–9) donates O2 of molecule number nine in cluster model (see Fig. 1c and Table 2).

All the electron density analyses at the BCP (a point between the hydrogen atom of donor group and acceptor atom involved in HB interaction) of HBs are performed using AIM 2000 code [74,75].

3. Results and discussion

This work is done to investigate the properties of the conventional N–H…O and unconventional S–H…O and S–H…S types of intermolecular HB interactions in the actual crystalline structures of L-Cysteine at 30 and 298 K by AIM analysis of charge density as well as DFT calculations of the EFG tensors at the sites of ^{17}O, ^{14}N, and ^{2}H nuclei. To include HB interactions effects, EFG calculations are performed for two molecular models including the monomer and nine-molecule cluster of L-Cysteine at both temperatures. Fig. 1 shows that L-Cysteine makes various intermolecular HBs in the solid phase, and then a cluster is created where the target molecule completely contribute to the HB interactions. To compare the calculated qcc and η_Q values with their given experimental values, one should consider the whole molecules in producing this cluster. The calculated EFG tensors are converted to the NQR parameters, qcc and η_Q, using Eqs. (1) and (2). The results are exhibited in Tables 3 and 4 and the available experimental data of qcc and η_Q for ^{14}N are also added. By a quick look at the calculated results of the monomer and the target molecule in the cluster, one can easily compare the capability of various nuclei contributing to HBs. In fact, the amount of changes in NQR parameters of a nucleus indicates its greater role among the other nuclei in contribution to HB. The ^{17}O, ^{14}N, and ^{2}H NQR parameters will be discussed in three sections, separately, where the results of B3LYP/6-311++G(d,p) are referred to. Finally, to clarify the presence of HB interactions and also rationalize the observed trends of calculated EFG tensors, wave functions of target L-Cysteine at 30 and 298 K are analyzed through AIM analysis which the results are exhibited in Tables 5 and 6 and are discussed in Section 3.5.

3.1. HBs in crystal structure of L-Cysteine

L-Cysteine crystallizes into two different polymorphs i.e. orthorhombic [30–33] and monoclinic [34–37]. In this study, the properties of HB interactions in the orthorhombic polymorph of L-Cysteine at 30 and 298 K are investigated. X-ray and neutron diffraction studies at both temperatures [30–32] revealed that carboxyl and amine groups are completely contribute to N–H…O type of HB interactions. N1 atom of target molecule in the cluster model contributes to HB interactions with molecules numbers 6, 7 and 8 (Fig. 1). Among these HB interactions, interaction with molecule number 8 located at (x+1/2,y,z), N1-H7…O2, has the shortest HB length (Table 2) and lies along the c direction (Fig. 2a and b). On the other hand, N1-H5…O1 HB interactions link molecules number 4 and 7 along a. The combination of these two HB interactions yields a layer composed of $R_4^4(16)$ ring motifs. The last of the N–H…O HB interactions at N1 site, N1-H6…O2, acts to link the layers together along

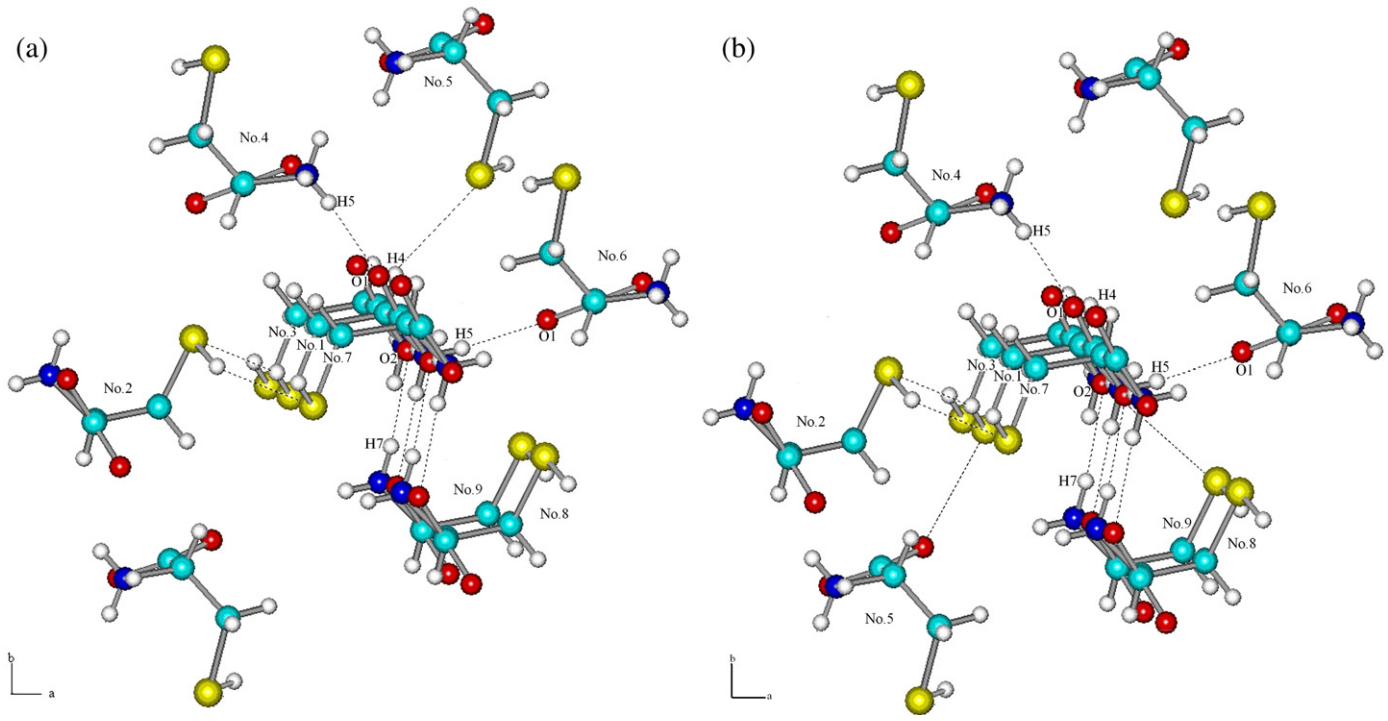

Fig. 2. (a) and (b) HB network of target molecule in nine-molecule cluster at 30 and 298 K, respectively. This view is along the c direction with a counterclockwise 5 degree rotation. Hydrogen-bonded layers in L-Cysteine are connected via N1-H7…O2 and N1-H5…O1 HB interactions. N1-H6…O2 HB acts to link these layers which lies in b direction and is not seen in this view.

the *b* direction (Fig. 2a and b). The computations show that N1-H6…O2 HB interactions undergo a significant change in bond lengths and NQR parameters of involved nuclei from 30 to 298 K where two other N–H…O HBs at N1 site do not change significantly (Tables 1–4). In the next sections, we will discuss more about these results.

Among carboxyl group oxygens, O1 with shorter covalent bond to carbon has only one HB interaction with H5 of molecule number four, while O2 has two N–H…O HBs and one S–H…O HB with molecules number 3 and 9 (Tables 1 and 2 and Fig. 1). X-ray and neutron diffraction [30–32] revealed that the difference in length between the two C–O bonds of carboxyl group is highly significant (see Table 1) and arises from the marked difference in the environments of the two atoms. Also, our DFT calculations indicate that qcc(^{17}O2) is 1 MHz greater than qcc(^{17}O1) at both temperatures, revealing the different chemical environments of the two oxygen nucleus. Koetzle et al. [31,32], by X-ray and neutron diffraction, showed that thiol group of L-Cysteine at 298 K is disordered in such a way as to form two intermolecular HB interactions; one with O2 at $3/2-x,2-y,1/2-z$ and one with S1 at $1/2-x,2-y,-1/2+z$. They suggest that disorder in the thiol group of L-Cysteine can be considered to involve both hydrogen and sulfur or just hydrogen. Also, they indicate that the model with order sulfur gives bond length and angles that are somewhat unusual and does not show the expected contraction of the H…S distance below the van der Waals contact distance of 2.75 Å. On the other hand, X-ray study of L-Cysteine at 30 K [30] showed that the structure is ordered with retention of the S–H…S HB interactions, $\mathbf{r}_{[S-H\ldots H]}$=2.66 Å and $\mathbf{r}_{[S\ldots S]}$=3.849 Å. The S–H…S interactions form an infinite hydrogen-bonded chain which zigzags along the *c* direction (Fig. 1). In the next sections we will discuss more about these interactions.

3.2. O-17 electric field gradient tensors

In this section, the calculated qcc and η_Q values of terminal carboxylic group oxygen nuclei (O1 and O2) are discussed see Table 3. By a quick look at the results, one can see some trends. First, the calculated ^{17}O EFG tensors of non hydrogen-bonded (monomer) model and hydrogen-bonded (cluster) one are different. Second, from the monomer to the cluster, the qcc values of both oxygen nuclei decrease, but, on the other hand, their η_Q values increase which reveal the participation of these nuclei in the intermolecular HB interactions. In fact, the magnitude of these changes for each nucleus depends on its contribution to the HB interactions. Therefore, more changes in each nucleus NQR parameters between the monomer and the target molecule in the cluster indicate its greater role among the other nuclei in contributing to HBs. Third, the qcc (^{17}O) and η_Q(^{17}O) results reveal that O1 and O2 do not have identical chemical environments in L-Cysteine. In other words, at both temperatures, qcc(^{17}O2) is 1 MHz greater than qcc(^{17}O1) while difference between the η_Q is almost negligible. Fourth, from 30 to 298 K, qcc(^{17}O) values of both oxygen nuclei (O1 and O2) decrease while their η_Q values have opposite tendency. Accurately, from 30 to 298 K, qcc(^{17}O1) and qcc (^{17}O2) reduce 0.07 and 0.08 MHz, respectively, whereas, η_Q values for both oxygen nuclei increase 0.03 units for the target molecule in the cluster. These changes for monomer are negligible.

Table 3 shows that qcc(^{17}O2) undergoes more reduction than qcc (^{17}O1) from monomer to the target molecule in cluster which reveal its contribution to stronger HB interactions in crystalline cluster at both temperatures. As can be seen from Fig. 1, the carboxylic group of the target molecule in cluster of L-Cysteine at both temperatures interacts with three neighboring molecules. O1 contributes to one N–H…O HB whereas O2 contributes to two N–H…O HBs. It should be noted that O2 has a weak non-classic S–H…O HB with molecule number 9 at 298 K. Because of proper intermolecular O…N distances in both clusters, $\mathbf{r}_{[O2\ldots N(1-9)]}$=2.75 Å, $\mathbf{r}_{[O2\ldots N(1-3)]}$=2.93 Å and $\mathbf{r}_{[O2\ldots S(1-9)]}$= 3.45 Å at 30 K, and $\mathbf{r}_{[O2\ldots N(1-3)]}$=3.02 Å and $\mathbf{r}_{[O2\ldots N(1-9)]}$=2.76 Å at 298 K, O2 of the target molecule contributes to stronger N–H…O HBs with molecules number 3 and 9 in the cluster. The results reveal that due to these contributions to HBs, qcc(^{17}O2) reduces 0.41 and 0.28 MHz from monomer to the target molecule in the cluster at 30 and 298 K, respectively. Based on these results, it is clear that, from 30 to 298 K, contribution of O2 nucleus to HB interactions is reduced which reveals that one or both of

the N–H…O HB interactions at O2 site undergo significant changes. The results of qcc(^{2}H) can clarify the amount of variation in each HB.

On the other hand, O1 of target molecule interacts with molecule 4 via N–H…O HB; approximately at both temperatures $\mathbf{r}_{[O1\ldots N(1-4)]}$=2.78 Å. Thus, because of participation in this interaction, qcc(^{17}O1) reduces 0.14 and 0.11 MHz from monomer to the target molecule in the cluster at 30 and 298 K, respectively, which are less significant than the reduction of qcc(^{17}O2); Δ(qcc(^{17}O2)=0.41 and 0.28 MHz from monomer to the target molecule in the cluster at 30 and 298 K, respectively. This trend reveals the major role of O2 in contribution to HB while that of O1 is significantly less. η_Q(^{17}O) is also affected by contribution of oxygen nuclei to HB interactions but not as dramatically as seen for qcc(^{17}O). η_Q values of O1 and O2 increase 0.11 and 0.08 from monomer to the target in cluster.

3.3. N-14 electric field gradient tensors

As a general trend seen from previous section, the amount of changes in the ^{17}O quadrupole coupling tensor depends directly on the participation of the nucleus in the intermolecular HB interactions. In this section, we focus on the results obtained for ^{14}N quadrupole coupling tensors; see Table 3. Two purposes are aimed in this discussion: first, to investigate the HB effects on the ^{14}N EFG tensors at the site of nitrogen nucleus and second, to compare the calculated results with experimental data.

A quick look at the results reveals the discrepancy between experimental and calculated qcc(^{14}N1) results of monomer at both temperatures. However, when HB effects are considered in the cluster, a good agreement is observed between experimental and calculated qcc(^{14}N1) results. As shown in Fig. 1, $^+$NH$_3$ terminal site of the target molecule in nine-molecule cluster of L-Cysteine interacts with three neighboring molecules through three N–H…O HB, $\mathbf{r}_{[N1\ldots O(1-6)]}$=2.77 Å, $\mathbf{r}_{[N1\ldots O(2-7)]}$=2.94 Å, and $\mathbf{r}_{[N1\ldots O(2-8)]}$=2.75 Å, at 30 K ,and $\mathbf{r}_{[N1\ldots O(1-6)]}$= 2.78 Å, $\mathbf{r}_{[N1\ldots O(2-7)]}$=3.02 Å, and $\mathbf{r}_{[N1\ldots O(2-8)]}$=2.74 Å, at 298 K. Thus, having a proper N…O distance, qcc(^{14}N1) increases 0.62 and 0.34 MHz from monomer to the target molecule in cluster at 30 and 298 K, respectively. HB also influences on the η_Q(^{14}N1) of the target molecule where the η_Q(^{14}N1) increases 0.33 and 0.21 units from monomer to the cluster at 30 and 298 K, respectively. The significant increase in qcc(^{14}N1) and η_Q values from monomer to the target molecule in cluster reveals the major contributions of nitrogen nuclei to strong N–H…O HBs in the cluster of L-Cysteine. The calculated qcc and η_Q values at the ^{14}N1 site of the target molecule at 298 K are 1.21 MHz and 0.39, respectively, which are in a good agreement with the experimental values at 298 K, qcc(^{14}N1)=1.22 MHz and η_Q=0.50 [56]. Thus, there is a good agreement between the calculated ^{14}N1 NQR parameters in the cluster model and experimentally reported values in the literature. However, since η_Q mainly depends on the orientation of the EFG tensors, less agreement between the calculated and experimental values of η_Q(^{14}N1) reveals that other effects, e.g. crystal effects, influence on the orientation of the EFG tensors at the site of ^{14}N1 in the experiments.

3.4. H-2 electric field gradient tensors

As discussed above, the EFG tensors at the sites of ^{17}O and ^{14}N nuclei are significantly influenced by contribution of the target molecule to HB interactions in the nine-molecule clusters of L-Cysteine at 30 and 298 K. This section discusses the influence of HB interactions on the EFG tensors at the site of ^{2}H nuclei in L-Cysteine which the evaluated NQR parameters are exhibited in Table 4. Comparison of the magnitudes of NQR parameters of Tables 3 and 4 reveals that these magnitudes for ^{2}H are less than those of ^{17}O and ^{14}N nuclei because the hydrogen nucleus feels a lower electron density comparing to those of ^{17}O and ^{14}N. However, since the EFG tensors are very sensitive to the electronic site of quadrupole nucleus, the influence of HB interactions on the EFG tensors at the sites of ^{2}H nuclei are observed in Table 4. Thus, as a general trend one can see in Table 4, qcc(^{2}H) values decease and η_Q(^{2}H) increase from non hydrogen-bonded (monomer) model to the hydrogen-bonded (cluster) one. It should be noted that for those nuclei that do not contribute to any HBs, this trend dose not exist.

For the target molecule at two mentioned temperatures, the hydrogens of $^+$NH$_3$ (H5, H6, and H7) contribute to N–H…O type of HB interactions, see Fig. 1. Due to the HBs, the ^{2}H EFG tensors at the amine site undergo significant changes from monomer to the target molecule in the cluster. qcc(^{2}H5), qcc(^{2}H6), and qcc(^{2}H7) reduce 24 (23.1), 16.5(10.6), and 27.3(26.6) kHz, respectively, at 30 and 298 K which the values out of the parentheses belong to 30 K. The results show that from 30 to 298 K, the N1-H7…O2 and N1-H5…O1 HBs remain approximately unchanged while N1-H6…O2 undergoes a significant change where Δ(qcc(^{2}H6)) feels 6 kHz reduction from 30 to 298 K. H1 of the target molecule L-Cysteine at 30 K contributes to one non-classic S1–H1…S(1–2) HB, while H1 of L-Cysteine at 298 K contributes to two non-classic S1–H1…S(1–2) and S1–H1…O(2–5) HBs, see Fig. 1. As a result, qcc(^{2}H1) reduces 9.7 and 14.7 kHz from monomer to the target molecule in the cluster at 30 and 298 K where η_Q remains almost unchanged. These results imply that the interactions with sulfur are stronger than those with oxygen. This is contrary to what would been accepted on the basis of electronegativity of the acceptor atoms. However, it can be noted that O2 is involved in two other N–H…O HBs, i.e. O2…H–N(1–3) and O2…H–N (1–9). Such interactions would decrease both the conformational mobility of O2 and its valence requirement thus reducing its availability as an acceptor for the thiol hydrogen. For C1 and C2 hydrogens, 11.1 and 4.5 kHz reduction in qcc values of H2 and H4 nuclei from monomer to the cluster at 30 K; Δ(qcc(^{2}H2))=11.1 kHz and Δ(qcc(^{2}H4))=4.5 kHz, stems from the contribution of those nuclei of target molecule to C–H…O and C–H…S HBs in cluster model. On the other hand, since these nuclei (H2 and H4) do not contribute to any HB in the cluster at 298 K, the EFG tensors at the sites of ^{2}H2 and ^{2}H4 of the target molecule are almost remained unchanged; Δ(qcc(^{2}H2))=1.3 kHz and Δ(qcc(^{2}H4))=0.9 kHz. H3 nucleus of target molecule also dose not contributes to HBs, thus, qcc(^{2}H3) values remains approximately unchanged from monomer to the cluster at both temperatures, Δ(qcc(^{2}H3))=1.5 and 0.6 kHz at 30 and 298 K, respectively.

Since hydrogen nuclei have poor electronic environment, the changes of η_Q are almost negligible in the cluster of L-Cysteine. However, η_Q increases just up to 0.05 from monomer to the target molecule in the cluster. By the results of these section it is clearly concluded that the role of amine hydrogens (H5, H6, and H7) to HB interactions in the cluster model of L-Cysteine is major while that of H2 and H4 is minor and almost negligible at both temperatures.

3.5. AIM analysis

AIM is a very useful tool in analyzing the hydrogen bond. The formation of HB is associated with the appearance of a BCP between the hydrogen atom of donor group and acceptor atom. Popelier and Bader [22] proposed a set of criteria for the existence of hydrogen bonding within the AIM formalism. Two criteria are connected with ρ_{BCP} and $\nabla^2\rho_{BCP}$ at BCP of two hydrogen bonded atoms which are in the range of 0.002–0.035 and 0.024–0.139 a.u., respectively.

For AIM analyses, wave functions of H-optimized crystalline structures of L-Cysteine at 30 and 298 K are calculated at the B3LYP/6-311++G** level from Gaussian 98 output. Then, the topological parameters in all BCPs of the HB interactions in L-Cysteine crystalline structures are evaluated by means of the AIM 2000 code [74,75] at the B3LYP/6-311++G** level. The most significant local topological properties at the BCPs for L-Cysteine crystalline structures at 30 and 298 K, namely: the density ρ_{BCP}, the Laplacian of density $\nabla^2\rho_{BCP}$, the three eigenvalues λ_1, λ_2 and λ_3, the ellipticity ε, the relationship between the perpendicular and parallel curvatures, $|\lambda_1|/\lambda_3$, in all the

relevant HBs are listed Tables 5 and 6. It is evident from these Tables that in all BCPs between the H atoms of HB donors and atoms of HB acceptors (H…O, H…N, and H…S) the values of ρ_{BCP} and $\nabla^2\rho_{BCP}$ are in the range of 0.0097–0.0451 and 0.0331–0.1618 a.u. for L-Cysteine at 30 K and 0.0101–0.0448 and 0.0403–0.1528 a.u. for L-Cysteine at 298 K, respectively. These values do not fall into the common accepted range for HBs mentioned above. However, relatively low ρ_{BCP} values, $\nabla^2\rho_{BCP}>0$, and $|\lambda_1|/\lambda_3<1$ for all BCPs of interactions indicate the general characteristics and presence of HB interactions.

From Tables 5 and 6, one can see some important points. H(7–1)…O(2–8) bond with having suitable topological parameters at its BCP, namely: $\rho_{BCP}=0.0450$, $\nabla^2\rho_{BCP}=0.1617$, $\varepsilon=0.0461$, can make strong HB interaction in comparison with other HBs, as a result the EFG tensors at the O2 and H7 sites should be affected more seriously. EFG calculations also show that qcc(^{17}O2) reduces 0.41 and 0.28 MHz and qcc(^{2}H7) reduces 27.3 and 26.6 kHz from monomer to the cluster (where the HBs exist) at 30 and 298 K, respectively. These AIM analyses and EFG calculations are in a good agreement with each other and geometrical parameters of H(7–1)…O(2–8) HB; $\mathbf{r}_{[N1\ldots O2]}=2.74$ Å, $\mathbf{r}_{[H\ldots O]}=1.65$ Å, and ∠N–H…O = 173.25° at 30 K, and $\mathbf{r}_{[N1\ldots O2]}=2.75$ Å, $\mathbf{r}_{[H\ldots O]}=1.71$ Å, and ∠N–H…O = 174.11° at 298 K (see Table 2).

As can be seen from the listed topological parameters in Tables 5 and 6, H(7–1)…O(2–8) HB interactions don't change considerably from 30 to 298 K ($\rho_{BCP}=0.0450$, $\nabla^2\rho_{BCP}=0.1617$ at 30 K, and $\rho_{BCP}=0.0448$, $\nabla^2\rho_{BCP}=0.1528$ at 298 K) which confirm the EFG calculation results for this interaction (Δqcc(^{2}H7) = 0.7 kHz from 30 to 298 K). For H(5–1)…O(1–6) HB, these conditions are also dominant where its topological parameters at BCP are: $\rho_{BCP}=0.0342$, $\nabla^2\rho_{BCP}=0.1451$, $\varepsilon=0.0148$ at 30 K, and $\rho_{BCP}=0.0318$, $\nabla^2\rho_{BCP}=0.1116$, $\varepsilon=0.0493$ at 298 K. These results are in a good agreement with H(5–1)…O(1–6) geometrical parameters; $\mathbf{r}_{[N1\ldots O1]}=2.77$ Å, $\mathbf{r}_{[H\ldots O]}=1.73$ Å, and ∠N–H…O = 165.67° at 30 K, and $\mathbf{r}_{[N1\ldots O2]}=2.78$ Å, $\mathbf{r}_{[H\ldots O]}=1.77$ Å, and ∠N–H…O = 164.54° at 298 K (see Table 2). Moreover, these values reveal that H(5–1)…O(1–6) HB interactions remain approximately unchanged from 30 to 298 K which rationalize the observed qcc(^{2}H5) trend (24 to 23.1 kHz from 30 to 298 K). Thus, at both mentioned temperatures, H(7–1)…O(2–8) and H(5–1)…O(1–6) HB interactions approximately have the same topological parameters. Moreover, low values of ε at BCPs of these interactions indicate stability of these HBs at both temperatures. However, H(6–1)…O(2–7) behavior is completely different from H(7–1)…O(2–8) and H(5–1)…O(1–6) HB interactions. In fact, from 30 to 298 K, ρ_{BCP} and $\nabla^2\rho_{BCP}$ values at the BCP of this HB interaction reduce approximately 50% (from 0.0222 to 0.0101 a.u. and from 0.0952 to 0.0403 a.u., respectively) which rationalize the observed trend of qcc(^{2}H6) values. The calculated Δqcc(^{2}H6) values are 16.5 and 10.6 kHz at 30 and 298 K, respectively (see Tables 4–6) which show approximately 60% variation. These AIM and EFG results are completely consistent with H(6–1)…O(2–7) geometrical parameters; $\mathbf{r}_{[N1\ldots O1]}=2.94$ Å, $\mathbf{r}_{[H\ldots O]}=1.86$ Å, and ∠N–H…O = 165.71° at 30 K, and $\mathbf{r}_{[N1\ldots O2]}=3.02$ Å, $\mathbf{r}_{[H\ldots O]}=2.06$ Å, and ∠N–H…O = 156.36° at 298 K (see Table 2). ε values also reveal that this HB interaction becomes instable from 30 to 298 K ($\varepsilon=0.0706$ and 0.0857 for 30 and 298 K, respectively).

Another interesting point occurs in H(1–1)…S(1–2) HB interactions which have topological parameters of $\rho_{BCP}=0.0141$, $\nabla^2\rho_{BCP}=0.0418$, and $\varepsilon=0.0529$ at 30 K; but, at 298 K, ρ_{BCP} and $\nabla^2\rho_{BCP}$ reduce to 0.0124 and 0.0388, and ε increases to 0.1176. In the pervious sections, based on the EFG calculations, it is observed that qcc(^{2}H1) reduces 9.7 and 14.7 kHz from monomer to the target molecule in the cluster at 30 and 298 K, respectively. ρ_{BCP} and $\nabla^2\rho_{BCP}$ changes and the contribution of H(1–1) to another HB interaction i.e. H(1–1)…O(2–5), justify the reduction of qcc(^{2}H1) at both temperatures and, particularly, its more reduction at 298 K with respect to 30 K.

Evaluated topological parameters for C–H…O and C–H…S HBs at 30 K are; $\rho_{BCP}=0.0102$ and $\nabla^2\rho_{BCP}=0.0359$, and $\rho_{BCP}=0.0097$ and $\nabla^2\rho_{BCP}=0.0331$, respectively. These low values of charge density at the BCPs of these interactions suggest that qcc(^{2}H2) and qcc(^{2}H4) should not reduce considerable. In agreement with this results obtained from AIM analyses, qcc(^{2}H2) and qcc(^{2}H4) reduce 11.1 and 4.5 kHz from monomer to the target in the cluster (see Table 4). At 298 K, the absence of BCPs at the H2 and H4 sites imply that HBs do not exist in these sites and clarifies the reduction in calculated Δqcc(^{2}H2) and Δqcc(^{2}H4) being 1.3 kHz and 0.9 kHz, respectively.

In summary, different contributions of various nuclei to HB interactions and observed trends of calculated EFG tensors are well justified by AIM analyses at the BCPs of these interactions.

4. Concluding remarks

In this paper, a systematic computational study on the HB interactions of L-Cysteine crystal structures is performed at 30 and 298 K by AIM analysis of charge density and DFT calculations of the EFG tensors at the sites of ^{17}O, ^{14}N, and ^{2}H nuclei in two one-molecule (monomer) and nine-molecule (cluster) models. Some results are:

1. EFG calculations results reveal that these tensors at the sites of oxygen, nitrogen, and hydrogen nuclei are influenced by HBs and are such appropriate parameters to characterize the properties of these interactions.
2. Since the nine-molecule model includes all possible contributions to HB for the target molecule, the calculated qcc and η_Q values at the ^{14}N1 site of the target molecule at 298 K are 1.21 MHz and 0.39 units, respectively, which are in a good agreement with the experimental values at 298 K, qcc(^{14}N1) = 1.22 MHz and $\eta_Q=0.50$.
3. For oxygen nuclei, the qcc(^{17}O) results reveal that O1 and O2 do not have identical chemical environments in L-Cysteine. At both mentioned temperatures, qcc(^{17}O2) is 1 MHz greater than qcc(^{17}O1).
4. O2 has the major role in contribution to HB interactions whereas the role of O1 is rather less. qcc(^{17}O1) reduces 0.14 and 0.11 MHz from monomer to the target molecule in the cluster at 30 and 298 K, respectively, which are less significant than the reduction in qcc (^{17}O2); Δqcc(^{17}O2) = 0.41 and 0.28 MHz at 30 and 298 K, respectively.
5. Among the hydrogen nuclei, HB has a remarkable influence on the EFG tensors at the amine site (H5, H6, and H7).
6. From 30 to 298 K, Δqcc(^{2}H6) undergoes a significant change while Δqcc(^{2}H) of other hydrogen nuclei are approximately negligible which reveal N-H6…O2 more affected than other N–H…O HB interactions. Also, AIM analyses at the BCP of this interaction show ρ_{BCP} and $\nabla^2\rho_{BCP}$ values at the BCP of this HB interaction reduce approximately 50% (from 0.0222 to 0.0101 a.u. and from 0.0952 to 0.0403 a.u., respectively) which justify the a significant change in Δqcc(^{2}H6).
7. Different contributions of various nuclei to HB interactions and observed trends of calculated EFG tensors are well rationalized by AIM analyses at the BCPs of these interactions.

Acknowledgments

The authors wish to gratefully thank the ACECR—Tehran branch for technical and financial supports. We thank Dr. Thomas F. Koetzle for sending X-ray and neutron diffraction data. We are also greatly indebted to Dr. Shant Shahbazian for his help in performing AIM analysis and Dr. Hamidreza Najafi for helpful advice and guidance in preparing this manuscript.

References

[1] G.A. Jeffrey, W. Saenger, Hydrogen Bonding in Biological Structures, Springer-Verlag, New York, 1991.
[2] A.V. Finkelstein, O.B. Ptitsyn, Protein Physics, Academic Press, London, 2002.
[3] Z. Gu, C.F. Ridenour, C.E. Bronniamann, T. Iwashita, A. McDermott, Hydrogen bonding and distance studies of amino acids and peptides using solid state 2D ^{1}H–^{13}C heteronuclear correlation spectra, J. Am. Chem. Soc. 118 (1996) 822–829.
[4] G.A. Kumar, M.A. McAllister, Theoretical investigation of the relationship between proton NMR chemical shift and hydrogen bond strength, J. Org. Chem. 63 (1998) 6968–6972.

[5] P. Cieplak, P.A. Kollman, On the use of electrostatic potential derived charges in molecular mechanics force fields. The relative solvation free energy of cis- and trans-N-methyl-acetamide, J. Comput. Chem. 12 (1991) 1232–1236.
[6] M. Strohmeier, D. Stueber, D.M. Grant, Accurate ^{13}C and ^{15}N chemical shift and ^{14}N quadrupolar coupling constant calculations in amino acid crystals: zwitterionic, hydrogen-bonded systems, J. Phys. Chem., A 107 (2003) 7629–7635.
[7] R.S. Lipsitz, Y. Sharma, B.R. Brooks, N. Tjandra, Hydrogen bonding in high-resolution protein structures: a new method to assess NMR protein geometry, J. Am. Chem. Soc. 124 (2002) 10621–10626.
[8] H.D. Lutz, Structure and strength of hydrogen bonds in inorganic solids, J. Mol. Struct. 646 (2003) 227–236.
[9] S. Scheiner, T. Kar, J. Pattanayak, Comparison of various types of hydrogen bonds involving aromatic amino acids, J. Am. Chem. Soc. 124 (2002) 13257–13264.
[10] C.H. Görbitz, Peptide structures, current opinion in solid state and material science 6 (2002) 109–116.
[11] C.H. Görbitz, Structures and conformational energies of amino acids in the zwitterionic, hydrogen-bonded state, J. Mol. Struct., Theochem 775 (2006) 9–17.
[12] H. Behzadi, N.L. Hadipour, M. Mirzaei, A density functional study of ^{17}O, ^{14}N and ^{2}H electric field gradient tensors in the real crystalline structure of α-glycine, Biophys. Chem. 125 (2007) 179–183.
[13] T.P. Das, E.L. Hahn, Nuclear quadrupole resonance spectroscopy, Academic Press, New York, 1958.
[14] E.A.C. Lucken, Nuclear Quadrupole Coupling Constants, Academic Press, London, 1969.
[15] E. Brunner, U. Sternberg, Solid-state NMR investigations on the nature of hydrogen bonds, Prog. Nucl. Magn. Reson. Spectrosc. 32 (1998) 21–57.
[16] R.F.W. Bader, Atoms In Molecules—A Quantum Theory, Oxford University Press, New York, 1990.
[17] P.L.A. Popelier, Atoms In Molecules—An Introduction, Pearson Education, Harlow, 2000.
[18] R.F.W. Bader, A quantum theory of molecular structure and its applications, Chem. Rev. 91 (1991) 893–928.
[19] M.T. Carroll, R.F.W. Bader, An analysis of the hydrogen bond in BASE–HF complexes using the theory of atoms in molecules, Mol. Phys. 65 (1988) 695–722.
[20] M.T. Carroll, C. Chang, R.F.W. Bader, Prediction of the structures of hydrogen-bonded complexes using the Laplacian of the charge density, Mol. Phys. 63 (1988) 387–405.
[21] R.F.W. Bader, C. Chang, Properties of atoms in molecules: electrophilic aromatic substitution, J. Phys. Chem. 93 (1989) 2946–2956.
[22] P.L.A. Popelier, R.F.W. Bader, The existence of an intramolecular C–H…O hydrogen bond in creatine and carbamoyl sarcosine, Chem. Phys. Lett. 189 (1992) 542–548.
[23] C.F. Matta, R.F.W. Bader, An atoms-in-molecules study of the genetically-encoded amino acids: I. effects of conformation and of tautomerization on geometric, atomic, and bond properties, Proteins: Struct. Funct. Genet. 40 (2000) 310–329.
[24] C.F. Matta, R.F.W. Bader, Atoms-in-molecules study of the genetically encoded amino acids. II. Computational study of molecular geometries, Proteins: Struct. Funct. Genet. 48 (2002) 519–538.
[25] C.F. Matta, R.F.W. Bader, Atoms-in-molecules study of the genetically encoded amino acids. III. Bond and atomic properties and their correlations with experiment including mutation-induced changes in protein stability and genetic coding, Proteins: Struct. Funct. Genet. 52 (2003) 360–399.
[26] H. Li, C. Wurrey, G.J. Thomas, Cysteine conformation and sulfhydryl interactions in proteins and viruses. 2. Normal coordinate analysis of the L-Cysteine side chain in model compounds, J. Am. Chem. Soc. 114 (1992) 7463–7469.
[27] H. Li, G.J. Thomas, Studies of virus structure by Raman spectroscopy. L-Cysteine conformation and sulfhydryl interactions in proteins and viruses. 1. Correlation of the Raman sulfur–hydrogen band with hydrogen bonding and intramolecular geometry in model compounds, J. Am. Chem. Soc. 113 (1991) 456–462.
[28] S.W. Raso, P.L. Clark, C. Haase-Pettingell, J. King, G.J. Thomas, Distinct cysteine sulfhydryl environments detected by analysis of Raman S–H markers of Cys→Ser mutant proteins, J. Mol. Biol. 307 (2001) 899–911.
[29] N.M. Gevondyan, A.M. Volynskaia, V.S. Gevondyan, Four free cysteine residues found in human IgG1 of healthy donors, Biochem. 71 (2006) 279–284.
[30] S.A. Moggach, S.J. Clark, S. Parsons, L-Cysteine-I at 30 K, Acta Crystallogr., Sect. E 61 (2005) 2739–2742.
[31] K.A. Kerr, J.P. Ashmore, Structure and conformation of orthorhombic L-Cysteine, Acta Crystallogr., Sect. B 29 (1973) 2124–2127.
[32] K.A. Kerr, J.P. Ashmore, T.F. Koetzle, A neutron diffraction study of L-Cysteine, Acta Crystallogr., Sect. B 31 (1975) 2022–2026.
[33] S.A. Moggach, D.R. Allan, S.J. Clark, M.J. Gutmann, S. Parsons, C.P. Pulham, L. Sawyer, High-pressure polymorphism in L-Cysteine: the crystal structures of L-Cysteine-III and L-Cysteine IV, Acta Crystallogr., Sect. B 62 (2006) 299–309.
[34] M.M. Harding, H.A. Long, The crystal and molecular structure of L-Cysteine, Acta Crystallogr., Sect. B 24 (1968) 1096–1102.
[35] B. Khawas, X-ray study of L-arginine HCl, L-Cysteine, DL-lysine and DL-phenylalanine, Acta Crystallogr., Sect B 27 (1971) 1517–1520.
[36] C.H. Görbitz, B. Dalhus, L-Cysteine, monoclinic form, redetermination at 120 K, Acta Crystallogr., Sect. C 52 (1996) 1756–1759.
[37] P. Luger, M. Weber, DL-Cysteine at 298 K, Acta Crystallogr., Sect. C 55 (1999) 1882–1885.
[38] T. Dudev, C. Lim, Factors governing the protonation state of cysteine in proteins: an ab initio/CDM study, J. Am. Chem. Soc. 124 (2002) 6759–6766.
[39] P.R. Lawrence, C. Thomson, A comparison of the results of PCILO and ab initio SCF calculations for the molecules glycine, L-Cysteine and N-acetyl-glycine, Theor. Chim. Acta 58 (1981) 121–124.
[40] D. Chakraborty, S. Manogaran, Ground state vibrational spectra of L-Cysteine and serine zwitterion: a theoretical prediction, J. Mol. Struct., Theochem 429 (1998) 31–40.
[41] P. Tarakeshwar, S. Manogaran, Vibrational frequencies of cysteine and serine zwitterions: an ab initio assignment, Spectrochim. Acta, Part A: Mol. Biomol. Spectrosc. 51 (1995) 925–928.
[42] S. Gronert, R.A.J. O' Hair, Ab initio studies of amino acid conformations. 1. The conformers of alanine, serine, and cysteine, J. Am. Chem. Soc. 117 (1995) 2071–2081.
[43] L. Schifer, K. Siam, V.J. Klimkowski, J.D. Ewbank, C.J. Van Alsenoy, Ab initio studies of structural features not easily amenable to experiment: Part 69. conformational analysis and structural study of cysteine, Mol. Struct. (Theochem) 204 (1990) 361–372.
[44] R. Maul, M. Preuss, F. Ortmann, K. Hannewald, F. Bechsedt, Electronic excitation of glycine, alanine, and cysteine conformers from first-principal calculations, J. Phys. Chem., A 111 (2007) 4370–4377.
[45] A. Pawlukojc, J. Leciejewicz, A.J. Ramirez-Cuesta, J. Nowicka-Scheibe, L-Cysteine: neutron spectroscopy, Raman, IR and ab initio study, Spectrochim, Acta A: Mol. Biomol. Spectrosc. 61 (2005) 2474–2481.
[46] S. Scheiner, T. Kar, G. Yanliang, Strength of the C^{α} H…O hydrogen bond of amino acid residues, J. Biol. Chem. 276 (2001) 9832–9837.
[47] F. Elmi, N.L. Hadipour, A study on the intermolecular hydrogen bonds of α-Glycylglycine in its actual crystalline phase using ab initio calculated ^{14}N and ^{2}H nuclear quadrupole coupling constants, J. Phys. Chem. A 109 (2005) 1729–1733.
[48] M. Mirzaei, N.L. Hadipour, K. Ahmadi, Investigation of C–H…O=C hydrogen-bonding interactions in crystalline thymine by DFT calculations of O-17, N-14 and H-2 NQR parameters, Biophys. Chem. 125 (2007) 411–415.
[49] A.R. Ghaderi, H. Sabzyan, N.L. Hadipour, Correlation between NQR parameters and residue size of aliphatic amino acids and their dimers, Biophys. Chem. 120 (2006) 62–70.
[50] D.T. Edmonds, P.A. Speight, Nitrogen quadrupole resonance in amino acids, Phys. Lett., A 34 (1971) 325–326.
[51] D.T. Edmonds, P.A. Speight, Nuclear quadrupole resonance of ^{14}N in pyrimidines, purines and their nucleosides, J. Magn. Reson. 6 (1972) 265–273.
[52] R. Blinc, M. Mali, R. Oserdkar, A. Prelesnik, J. Seliger, I. Zupancic, L. Ehrenberg, ^{14}N spectroscopy of some amino acids and nucleic bases via double resonance in the laboratory frame, J. Chem. Phys. 57 (1972) 5087–5093.
[53] D.T. Edmonds, Nuclear quadrupole double resonance, Phys. Rep. 29 (1977) 233–290.
[54] D.T. Edmonds, C.P. Summers, ^{14}N pure quadrupole resonance in solid amino acids, J. Magn. Reson. 12 (1973) 134–142.
[55] K.J. Pike, V. Lemaitre, A. Kukol, T. Anupold, A. Samoson, A.P. Howes, A. Watts, M.E. Smith, R. Dupree, Solid state ^{17}O NMR of amino acids, J. Phys. Chem., B 108 (2004) 9256–9263.
[56] T. Giavani, H. BildsØe, J. Skibsted, H.J. Jakobsen, A solid-state ^{14}N magic-angle spinning NMR study of some amino acids, J. Magn. Reson. 166 (2004) 262–272.
[57] M. Mirzaei, N.L. Hadipour, An investigation of hydrogen-bonding effects on the nitrogen and hydrogen electric field gradient and chemical shielding tensors in the 9-methyladenine real crystalline structure: a density functional theory study, J. Phys. Chem., A 110 (2006) 4833–4838.
[58] R. Ida, M.D. Clerk, G. Wu, Influence of N–H…O and C–H…O hydrogen bonds on the ^{17}O NMR tensors in crystalline uracil: computational study, J. Phys. Chem., A 110 (2006) 1065–1071.
[59] S. Dong, R. Ida, G. Wu, A combined experimental and theoretical ^{17}O NMR study of crystalline urea: an example of large hydrogen-bonding effects, J. Phys. Chem. 104 (2000) 11194–11202.
[60] G. Wu, S. Dong, R. Ida, N. Reen, A solid state ^{17}O nuclear magnetic resonance study of nucleic acid bases, J. Am. Chem. Soc. 124 (2002) 1768–1776.
[61] M. Torrent, D.G. Musaev, K. Morokuma, Calculation of nuclear quadrupole parameters in imidazole derivatives and extrapolation to coenzyme B12. a theoretical study, J. Phys. Chem., B 103 (1999) 8618–8627.
[62] M. Aghazadeh, M. Mirzaei, Hydrogen bond interactions in sulfamerazine: DFT study of the O-17, N-14 and H-2 electric field gradient tensors, Chem. Phys. 351 (2008) 159–162.
[63] A.G. Nozad, H. Najafi, S. Meftah, M. Aghazadeh, A systematic study on hydrogen bond interactions in sulfabenzamide: DFT calculations of the N-14, O-17 and H-2 NQR parameters, Biophys. Chem. 139 (2009) 116–122.
[64] M.J. Frisch, G.W. Trucks, H.B. Schlegel, G.E. Scuseria, M.A. Robb, J.R. Cheeseman, V.G. Zakrzewski, J.A. Montgomery Jr., R.E. Stratmann, J.C. Burant, S. Dapprich, J.M. Millam, A.D. Daniels, K.N. Kudin, M.C. Strain, O. Farkas, J. Tomasi, V. Barone, M. Cossi, R. Cammi, B. Mennucci, C. Pomelli, C. Adamo, S. Clifford, J. Ochterski, G.A. Petersson, P.Y. Ayala, Q. Cui, K. Morokuma, D.K. Malick, A.D. Rabuck, K. Raghavachari, J.B. Foresman, J. Cioslowski, J.V. Ortiz, A.G. Baboul, B.B. Stefanov, G. Liu, A. Liashenko, P. Piskorz, I. Komaromi, R. Gomperts, R.L. Martin, D.J. Fox, T. Keith, M.A. Al-Laham, C.Y. Peng, A. Nanayakkara, C. Gonzalez, M. Challacombe, P.M.W. Gill, B. Johnson, W. Chen, M.W. Wong, J.L. Andres, C. Gonzalez, M. Head-Gordon, E.S. Replogle, J.A. Pople, Gaussian 98, Gaussian Inc., Pittsburgh, PA, 1998.
[65] M. Köster, P. Calaminici, N. Russo, Nuclear quadrupole coupling constants from the Gaussian density-functional method, Phys. Rev., A 53 (1996) 3865–3868.
[66] G. De Luca, N. Russo, A.M. Köster, P. Calaminici, K. Jug, Density functional theory calculations of nuclear quadrupole coupling constants with calibrated ^{17}O quadrupole moments, Mol. Phys. 97 (1999) 347–354.
[67] E. Sicilia, G. De Luca, S. Chiodo, N. Russo, P. Calaminici, A.M. Köster, K. Jug, Density functional calculations of nuclear quadrupole coupling constants with calibrated ^{14}N quadrupole moments, Mol. Phys. 99 (2001) 1039–1051.
[68] A.D. Becke, Density-functional thermochemistry. III. The role of exact exchange, J. Chem. Phys. 98 (1993) 5648–5652.
[69] C. Lee, W. Yang, R.G. Parr, Development of the colle–salvetti correlation–energy formula into a functional of the electron density, Phys. Rev., B 37 (1988) 785–789.

[70] J.P. Perdew, Y. Wang, Accurate and simple analytic representation of the electron–gas correlation energy, Phys. Rev., B 45 (1992) 13244–13249.
[71] R.G. Parr, W. Yang, Density–Functional Theory of Atoms and Molecules, Oxford Univ. Press, Oxford, 1989.
[72] A.D. McLean, G.S. Chandler, Contracted Gaussian basis sets for molecular calculations. I. Second row atoms, $Z=11–18$, J. Chem. Phys. 72 (1980) 5639–5644.
[73] P. Pyykkö, Spectroscopic nuclear quadrupole moment, Mol. Phys. 99 (2001) 1617–1629.
[74] F. Biegler-König, J. Schönbohm, D. Bayles, AIM2000— a program to analyze and visualize atoms in molecules, J. Comput. Chem. 22 (2001) 545–559.
[75] F. Biegler-König, J. Schönbohm, An update to the AIM2000— program for atoms in molecules, J. Comput. Chem. 23 (2002) 1489–1494.